Evidence for Chaotic Behavior during the Yielding of a Soft Particle Glass

David C. Venerus,* Otar Machabeli, Daniela Bushiri, and Seyed Mahmoud Arzideh
Department of Chemical and Materials Engineering, New Jersey Institute of Technology, Newark, New Jersey 07102, USA

(Received 25 February 2022; accepted 20 July 2022; published 4 August 2022)

Materials comprised of deformable particles such as microgels and concentrated emulsions and foams display complex rheological behavior that includes a yielding transition from an elastic solid to viscous fluid. Most studies of this class of soft matter involve shear flows, and only a handful report both shear and normal stresses. We present measurements of the shear stress and two normal stress differences for a microgel subjected to constant shear rate flows. The shear stress evolves through the yield point in a manner indicative of simple yield stress fluid behavior. Prior to yielding, the normal stress differences are immeasurable; beyond the yield point, they evolve in a reproducibly chaotic manner.

DOI: 10.1103/PhysRevLett.129.068002

Yield stress fluids are an important class of soft matter that display complex rheological behaviors. Materials such as microgels [1], foams [2], and concentrated suspensions [3,4] and emulsions [5], which are sometimes referred to as soft particle glasses, often display yield stress fluid behavior. Common examples of yield stress fluids include foods, personal care products, mud, and cement. The rheological behavior of yield stress fluids, which is crucial to their function, is often described as elastoviscoplastic (EVP). Prior to yielding, EVP materials behave like an elastic solid, and after yielding they behave like a viscous fluid. During the past two decades, there has been a surge in research on the rheological behavior of this important class of soft matter, and several excellent reviews are available [6–9].

So-called *simple* yield stress fluids [9–13] display nonthixotropic rheological behavior; that is, the stress depends only on the applied strain rate and not on the prior deformation history. Several systems including foams, emulsions, and dispersions appear to behave as simple yield stress fluids [10–14]. The most widely studied simple yield stress fluid is a microgel known as Carbopol [14–17], which is a dispersion of swollen, cross-linked polyacrylic acid particles having a diameter of $\sim 10\ \mu$m. A common test for simple yield stress behavior is to subject the sample to a shear stress σ that is cycled from low to high to low values and the shear rate $\dot{\gamma}$ is measured—the absence of hysteresis over the cycle indicates simple yield stress fluid behavior. In principal, both experimental and theoretical studies of simple yield stress fluids are more straightforward compared to thixotropic fluids.

A critical issue in yield stress fluid rheology is the determination of the stress (or strain) at which the solid-to-fluid transition occurs, or the yield point [18–20]. Typically, the yield point is quantified by a critical stress called the yield stress τ_y below which the material displays solid elastic behavior. One approach to determine the (dynamic) yield stress τ_y is to subject the sample to a range of shear stresses σ and identify the shear stress where the measured the shear rate $\dot{\gamma}$ vanishes. Alternatively, the sample is subjected to a constant shear rate $\dot{\gamma}$ and the point where the shear stress σ deviates from a linear dependence on strain $\gamma(=\dot{\gamma}t)$, or goes through a maximum, determines the (static) yield stress τ_y.

The preponderance of rheological studies on yield stress fluids involve simple shear deformations, and, with a few exceptions, only the shear stress σ is considered. However, complex fluids subjected to shear deformations develop normal stresses [21–24], which result from anisotropy of the fluid microstructure. For an incompressible fluid subjected to simple shear flow with shear rate $\dot{\gamma} = \partial v_1/\partial x_2$, the extra stress tensor $\boldsymbol{\tau}$ is completely described by the shear stress $\sigma = \tau_{12} = \tau_{21}$ and the first $N_1 = \tau_{11} - \tau_{22}$ and second $N_2 = \tau_{22} - \tau_{33}$ normal stress differences. While notoriously difficult to measure, it is well established that $N_1 > 0$ and $-N_2 \ll N_1$ for polymeric liquids [21,22], while the picture is less clear for concentrated hard-sphere suspensions [25,26]. By contrast, the evolution of normal stresses in soft jammed matter remains virtually unexplored.

In this Letter, we report new and somewhat surprising results that illuminate the behavior of normal stresses during the yielding of a soft particle glass in shear deformations. The shear stress and two normal stress differences (σ, N_1, and N_2) are measured for a Carbopol microgel that is usually classified as a "simple" yield stress fluid, so that the complete state of stress is known prior to, at, and beyond the yield point. Great effort is taken to eliminate artifacts in these measurements, including one that appears to have previously been overlooked. We further show that the designation of yield stress fluids as simple based solely on shear stress may be inadequate.

The small number of studies [27–33] that have reported normal stresses for yield stress fluids show significant variability. For Carbopol microgels and foams, several studies report $N_1 > 0$ [28–32] and $N_1 - N_2 > 0 (N_2 < 0)$ in constant shear rate and large amplitude oscillatory shear deformations [31,32]. However, $N_1 < 0$ and $N_1 - N_2 < 0$ have also been reported for microgels in constant stress flows [33]. It is noteworthy that in several studies corrections were applied for signal drift and capillary stresses to ensure $N_1 > 0$ at small shear rates [31,32].

The scarcity of normal stress data on yield stress fluids severely limits attempts to understand the rheological behavior of EVP fluids. Normal stresses are important to the function of yield stress fluids, which are often subject to complex deformations [34–37]. Thus far, the classification of simple yield stress fluid behavior is based entirely on the shear stress σ. An incomplete characterization of the state of stress in yield stress fluids also hinders attempts to develop both microstructural models and phenomenological rheological constitutive equations [38–44].

A simple model for EVP rheological behavior in isochoric, simple shear flows can be written as

$$\sigma = G\gamma, \quad \text{for } \sigma < \tau_y, \tag{1}$$

$$\sigma = \tau_y + K\dot{\gamma}^m, \quad \text{for } \sigma \geq \tau_y, \tag{2}$$

which has four parameters: the shear modulus G, the viscosity coefficient K, the power-law index m, and the yield stress τ_y. In the limit $G \to \infty$, (2) is known as the Herschel-Bulkley model [45], and if $m = 1$ and $K \to \eta$, the Bingham model [46] with viscosity η is obtained. The model involving both elastic (1) and viscous (2) behavior is associated with Oldroyd [47].

The most widely used yielding criterion for yield stress fluids is the von Mises yielding criterion: $\sqrt{\mathrm{II}_{\tau'}} \geq \tau_y$, where $\mathrm{II}_{\tau'} = 1/2(\boldsymbol{\tau}' : \boldsymbol{\tau}')$ is the second invariant of the deviatoric stress tensor: $\boldsymbol{\tau}' = \boldsymbol{\tau} - \mathrm{tr}(\boldsymbol{\tau})/3\boldsymbol{\delta}$. For simple shear flows, the von Mises yielding criterion is given by

$$\sqrt{\mathrm{II}_{\tau'}} = \sqrt{\sigma^2 + (N_1^2 + N_1 N_2 + N_2^2)/3} \geq \tau_y. \tag{3}$$

The EVP model in (1) and (2) implies $N_1 = N_2 = 0$ so that $\sqrt{\mathrm{II}_{\tau'}} = \sigma$. Several studies have attempted to evaluate the von Mises yielding criterion by considering elongational [48–50] and complex (nonviscometric) [51,52] flows. For example, in simple elongational flow with strain rate $\dot{\epsilon} = \partial v_1/\partial x_1$, $\sqrt{\mathrm{II}_{\tau'}} = \sigma^u/\sqrt{3}$, where $\sigma^u = \tau_{11} - \tau_{22}$ is the tensile stress. Hence, according to the von Mises criterion, the tensile stress σ^u at the yield point in simple elongation is a factor of $\sqrt{3}$ larger than the yield stress in simple shear. These flows are a challenge to realize experimentally and/or are difficult to interpret, however, which has resulted in somewhat inconclusive results [48–53]. Moreover, most attempts to test the von Mises yielding criterion ignore contributions of N_1 and N_2 to the yield stress criterion given in (3).

In the present study, experiments were conducted in both cone-plate and parallel-plate geometries. For cone-plate flow, the shear rate is approximately uniform throughout the sample $\dot{\gamma} = \Omega/\beta$, where Ω is the angular velocity of the cone and $\beta (\ll 1)$ is the cone angle. The shear stress σ and first normal stress difference N_1 can be obtained from the torque M and axial force F exerted on the plate [21,22]. For parallel-plate flow, the shear rate has a linear dependence on radial position, and the shear rate at the edge of the plate is $\dot{\gamma}_R = \Omega R/H$, where R is the plate radius and $H (\ll R)$ is the plate separation. The shear stress σ and difference of normal stress differences $N_1 - N_2$ are determined from the torque M and axial force F exerted on the plate using well-known relations [21,22] (see Supplemental Material [54]).

All results presented here are for a 1.0% Carbopol microgel. This material and the procedure used to prepare it (see Supplemental Material [54]) are similar to those described in the literature for making simple yield stress fluids [10–12,16,17,32,33,42]. Cone-plate and plate-plate fixtures were coated with sandpaper (400 grit, ~20 μm roughness) to mitigate slip. Experiments were performed at room temperature $22 \pm 1\,^{\circ}\mathrm{C}$ with the sample inside an environmental chamber having a water-saturated sponge to minimize evaporation. Rheological data were obtained using two instruments: an MCR302 (Anton Paar) controlled stress rheometer and an RMS800 (Rheometrics, Inc.) controlled strain rheometer. Samples were subjected to a preshear consisting of the following sequence: $\dot{\gamma}$ (or $\dot{\gamma}_R$) $= 1.0, -1.0, 1.0, -1.0\ \mathrm{s}^{-1}$ each for 100 s and then allowing 30 min before rheological tests were performed.

A parallel-plate geometry ($R = 25.0$ mm, $H = 2.0$ mm) was employed on the MCR302 to measure the complex modulus $G^*(\omega) = G'(\omega) + \imath G''(\omega)$, where $G'(\omega)$ and $G'(\omega)$ are the storage and loss moduli, respectively, in small-amplitude oscillatory shear over a range of frequencies ω. This device was also used with a cone-plate geometry ($R = 25.0$ mm, $\beta = 0.1$) to conduct experiments where $\dot{\gamma}$ $[\mathrm{s}^{-1}]$ was ramped from $0.004 \to 10 \to 0.004$ and the steady-state shear stress σ was measured. The results of this test are shown in Fig. 1, where the absence of hysteresis in the flow curve indicates simple yield stress fluid behavior [9–13]. This figure includes a fit of the Herschel-Bulkley model (2) to the shear stress σ giving a (dynamic) yield stress $\tau_y = 112$ Pa. The inset shows the dynamic moduli $G'(\omega)$ and $G'(\omega)$ from which we estimate the shear modulus $G = G'(0.1\ \mathrm{rad/s}) = 780$ Pa.

Constant shear rate experiments were made on the RMS800 with cone-plate fixtures ($R = 25.0$ mm, $\beta = 0.1$ rad) and parallel-plate fixtures ($R = 25.0$ mm, $H = 2.0$ mm) for $\dot{\gamma}$ (or $\dot{\gamma}_R$) $= 0.01, 0.1, 1.0\ \mathrm{s}^{-1}$ to a strain of $\gamma = \dot{\gamma}t$ (or $\gamma_R = \dot{\gamma}_R t$) $= 2.0$. For each shear rate and geometry, data were collected for at least ten repeat

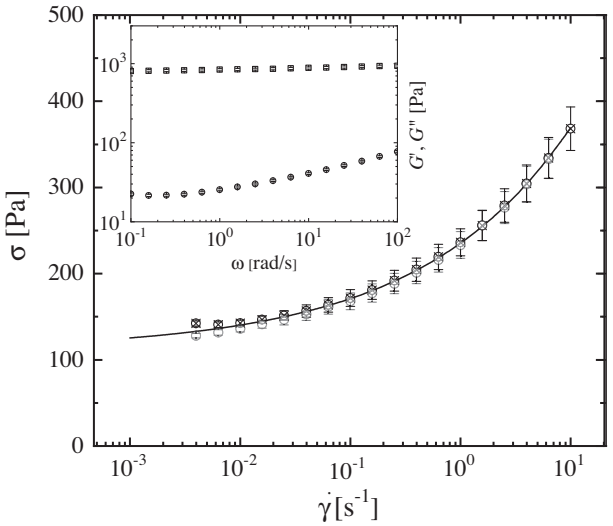

FIG. 1. Flow curve for 1% Carbopol microgel measured in cone-plate flow showing shear stress σ ($\dot{\gamma}$ increasing ⊗, decreasing ○) versus shear rate $\dot{\gamma}$. The solid curve is a fit of (2) with $\tau_y = 112$ Pa, $K = 123$ Pa s^m, and $m = 0.32$. The inset shows dynamic moduli G'(○) and G'(□) versus frequency ω.

experiments that involved multiple sample loadings and alternating the sign of the applied shear rate. We note that, in conducting these experiments, great care was taken to minimize the effects of transducer axial compliance on normal stress difference measurements [56–64], which does not appear to be the case in previous studies [31–33] reporting normal stresses for yield stress fluids (see Supplemental Material [54]).

Results from constant shear rate experiments are shown in Fig. 2. Shear stress σ and first normal stress difference N_1 versus strain γ for shear rate $\dot{\gamma} = 0.1$ s^{-1} for 12 repeat cone-plate flow experiments are shown in Fig. 2(a). From this figure, we see that σ initially displays a linear dependence on γ followed by a monotonic approach to a constant (steady) value and also that the repeat experiments have a high degree of reproducibility with variations that are comparable to the experimental uncertainty. The first normal stress difference N_1 shown in Fig. 2(a) is immeasurably small for $\gamma \lesssim 0.15$, after which it evolves in a rather chaotic manner with variations that are much larger than the uncertainty of the measurement. It is important to emphasize that, for each of the 12 repeat experiments shown in this figure, σ and N_1 were measured *simultaneously*. In other words, looking only at σ, which show a high degree of reproducibility, one would conclude that this material is a simple yield stress fluid, while the chaotic behavior of N_1 would suggest otherwise.

The shear stress $2M/\pi R^3$ and normal stress $2F/\pi R^2$ versus strain γ_R for shear rate $\dot{\gamma}_R = 0.1$ s^{-1} for ten repeat parallel-plate flow experiments are shown in Fig. 2(b). From this figure, we see that the shear stress data are qualitatively similar to σ data in Fig. 2(a) and show good reproducibility. The normal stress data in Fig. 2(b) are immeasurably small for $\gamma_R \lesssim 0.15$ and then evolve to a significant magnitude in a chaotic manner. Again, it is important to emphasize that, for each of the ten repeat experiments shown in Fig. 2(b), $2M/\pi R^3$ and $2F/\pi R^2$ were measured simultaneously. Previous studies [28,30,32,33] reporting normal stress data on similar Carbopol microgels do not mention the reproducibility of these measurements nor if they were chaotic in nature.

In Fig. 2(c), we show the average shear stress σ and first normal stress difference N_1 from the data in Fig. 2(a) and the shear stress σ and difference of normal stress differences $N_1 - N_2$ computed (see Supplemental Material [54]) from the average of the data in Fig. 2(b), versus strain γ. The good agreement of the shear stress σ from cone-plate and parallel-plate geometries suggests that slip is not present in the experiments. Prior to yielding $\gamma \lesssim 0.15$, it appears that both normal stress differences are effectively zero. At and beyond the yield point $\gamma \gtrsim 0.15$, in spite of the chaotic nature of the repeat experiments for the normal stress measurements, it appears that $N_1 \sim 0$ while $N_1 - N_2 > 0$, which means $N_2 < 0$. The results presented in Fig. 2 appear to be the first showing the evolution of the

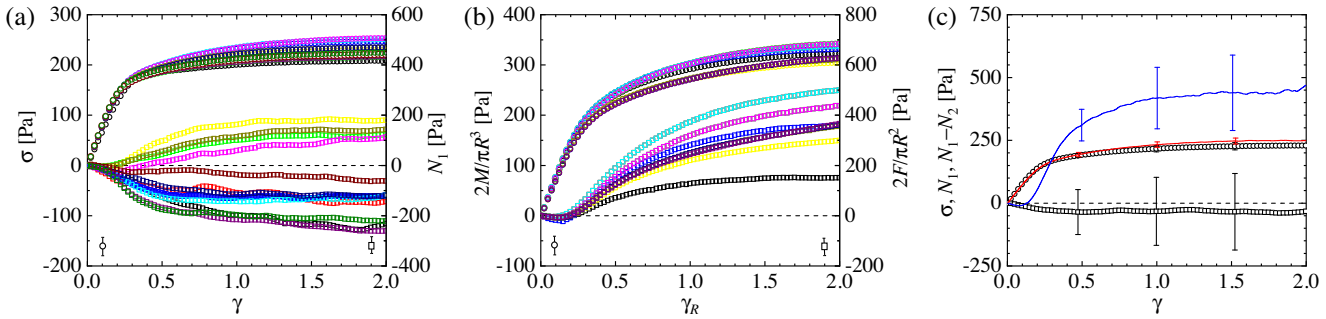

FIG. 2. Shear and normal stresses versus strain $\gamma(\gamma_R)$ for 1% Carbopol microgel for constant shear rate $\dot{\gamma} = \dot{\gamma}_R = 0.1$ s^{-1}. (a) σ (○) and N_1 (□) from cone-plate flow for 12 repeat experiments (different color symbols); (b) $2M/\pi R^3$ (○) and $2F/\pi R^2$ (□) from parallel-plate flow for ten repeat experiments (different color symbols); (c) average σ (○) and N_1 (□) from (a) and computed σ (red curve) and $N_1 - N_2$ (blue curve) from averages of the data in (b). Symbols with error bars represent uncertainty of measured quantities in (a) and (b), and error bars in (c) represent standard deviations from repeat experiments or estimated errors in computed quantities.

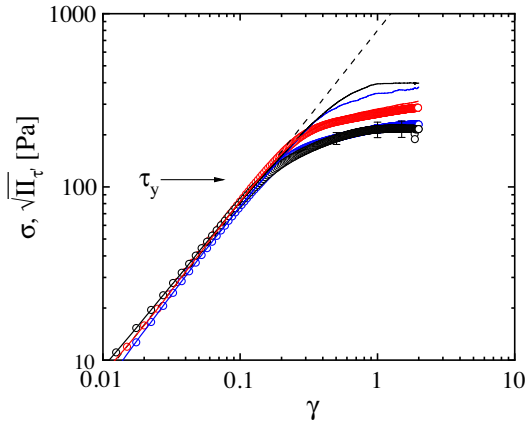

FIG. 3. Shear stress σ (○) and $\sqrt{\Pi_{\tau'}}$ (curves) versus strain γ for shear rates $\dot{\gamma}$ [s^{-1}] = 0.01 (black), 0.10 (blue), and 1.0 (red). The dashed line is linear elastic solid prediction (1) with $G = 780$ Pa; the arrow indicates the yield stress $\tau_y = 112$ Pa obtained from Fig. 1.

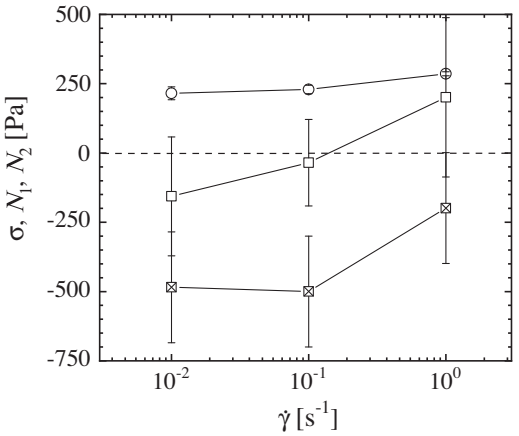

FIG. 4. Steady state σ (○), N_1 (□), and N_2 (⊠) versus shear rate $\dot{\gamma}$ for 1% Carbopol microgel. Error bars on symbols represent standard deviation in measured and computed quantities.

normal stress differences in a yield stress fluid with strain (time) as the material undergoes a yielding transition. Results obtained at two other shear rates $\dot{\gamma}(\text{or}\,\dot{\gamma}_R) = 0.01, 1.0\ s^{-1}$ display qualitatively similar behavior to that shown in Fig. 2 (see Supplemental Material [54]).

Shear stress σ versus strain γ results for three shear rates $\dot{\gamma}$ [s^{-1}] = 0.01, 0.1, 1.0 are shown in Fig. 3. For $\gamma \lesssim 0.15$, the shear stress σ is independent of $\dot{\gamma}$ and has a linear dependence on γ. Also shown in this figure is $\sqrt{\Pi_{\tau'}}$ computed from (3) using the results in Fig. 2, which is consistent with σ for $\gamma \lesssim 0.15$ as expected, since both N_1 and N_2 are small for this strain level. Hence, prior to yielding, the behavior of the Carbopol microgel yield stress fluid can be described as a Hookean elastic solid (1). These results also suggest that the von Mises yield criterion is simply $\sigma \geq \tau_y$, which is consistent with those in Refs. [31,32,48–51] but contradicts those of Refs. [33,52,53]. For $\gamma \sim 0.15$, at which point the shear stress σ coincides with the yield stress $\tau_y = 112$ Pa obtained from the flow curve in Fig. 1, the shear stress deviates from $\sigma \propto \gamma$, and the normal stress differences N_1 and N_2 develop so that $\sqrt{\Pi_{\tau'}}$ deviates from σ. The results in Figs. 2 and 3 indicate that normal stresses in yield stress fluids develop only at the yielding point and are unimportant prior to yielding.

Figure 4 shows steady-state, postyield, values of the shear stress σ and normal stress differences N_1 and N_2 versus shear rate $\dot{\gamma}$. Within the standard deviation of the repeat experiments, $N_1 \sim 0$, but the data in this figure suggest a sign change over this range of shear rates. In spite of the large uncertainty, results for the second normal stress difference are more clear $N_2 < 0$. In relation to previous studies with normal stress measurement on similar Carbopol microgels, $N_1 > 0$ at shear rates $\dot{\gamma} \gtrsim 1\ s^{-1}$ has been reported [28,30,32]. The results of Ref. [32] also show $N_2 < 0$, and, for $\dot{\gamma} \lesssim 1\ s^{-1}$, N_1 data have large standard deviations obtained from (two) repeat experiments and appear to decrease with decreasing shear rate. Experimental and simulation results for concentrated hard-sphere suspensions [26,65] and experimental results for emulsions [31,66] show similar behavior, that is, small N_1 and $N_2 < 0$.

The experimental results presented in this Letter are strong evidence that the yielding transition for soft particle glasses in constant shear rate flow triggers the growth and *chaotic* evolution of normal stresses, while the shear stress evolves in a reproducible manner. We now address the question of how these unexpected macroscopic observations are related to material microstructure and its flow-induced change. Prior to each test, the sample is subjected to a (pre)shear deformation and allowed to rest for at least 30 min, which determines the initial microstructure (state) for a subsequent test. At small strains $\gamma \lesssim 0.15$, the shear stress σ results from the elastic deformation of the jammed particles that are trapped in their cages. The absence of normal stresses for $\gamma \lesssim 0.15$ suggests that the particles initially have an isotropic distribution. As the material undergoes a yielding transition for $\gamma > 0.15$, the particles are released from their cages, allowing the microstructure to become anisotropic, which results in normal stresses. The initial microstructure of the microgel examined in this work appears to be relatively unimportant to the evolution of the shear stress σ. The normal stress differences N_1 and N_2, however, which evolve in a chaotic manner, appear to be highly sensitive to the initial state of the microstructure. This picture is consistent with particle-based simulation results for a system composed of deformable particles [39,67,68] and those based on dissipative particle dynamics [69].

Connections have been made between a yielding transition and chaotic behavior in systems comprised of both

hard [70] and soft [71] particles. Microscopic quantities such as particle positions reveal a transition from reversible to irreversible (nondiffusive to diffusive) dynamics above a critical strain in oscillatory shear. Indeed, at the critical strain, the particle mean-square displacement or diffusivity can increase by several orders of magnitude. The results presented here appear to be the first to show how this transition is manifested in the chaotic evolution of normal stresses in a soft particle glass. Further studies on additional systems including emulsions and foams would shed light on the generality of this phenomenon.

*venerus@njit.edu

[1] P. Coussot, Soft Matter **3**, 528 (2007).
[2] *Foams: Theory, Measurements, and Applications*, edited by R. K. Prud'homme and S. A. Khan (Taylor & Francis Group, New York, 2017).
[3] A. Singh, S. Pednekar, J. Chun, M. M. Denn, and J. F. Morris, Phys. Rev. Lett. **122**, 098004 (2019).
[4] *Theory and Applications of Colloidal Suspension Rheology*, edited by N. J. Wagner and J. Mewis (Cambridge University Press, Cambridge, England, 2021).
[5] T. G. Mason, J. Bibette, and D. A. Weitz, J. Colloid Interface Sci. **179**, 439 (1996).
[6] N. J. Balmforth, I. A. Frigaard, and G. Ovarlez, Annu. Rev. Fluid Mech. **46**, 121 (2014).
[7] P. Coussot, J. Non-Newtonian Fluid Mech. **211**, 31 (2014).
[8] A. Malkin, V. Kulichikhin, and S. Ilyin, Rheol. Acta **56**, 177 (2017).
[9] D. Bonn, M. M. Denn, L. Berthier, T. Divoux, and S. Manneville, Rev. Mod. Phys. **89**, 035005 (2017).
[10] P. C. F. Møller, A. Fall, V. Chikkadi, D. Derks, and D. Bonn, Phil. Trans. R. Soc. A **367**, 5139 (2009).
[11] G. Ovarlez, S. Cohen-Addad, K. Krishon, J. Goyon, and P. Coussot, J. Non-Newtonian Fluid Mech. **193**, 68 (2013).
[12] M. Dinkgreve, M. Fazilati, M. M. Denn, and D. Bonn, J. Rheol. **62**, 773 (2018).
[13] I. Frigaard, Curr. Opin. Colloid Interface Sci. **43**, 80 (2019).
[14] A. Magnin and J. M. Piau, J. Non-Newtonian Fluid Mech. **36**, 85 (1990).
[15] J. M. Piau, J. Non-Newtonian Fluid Mech. **144**, 1 (2007).
[16] P. R. Varges, C. M. Costa, B. S. Fonseca, M. F. Naccache, and P. R. de Souza Mendes, Fluids **4**, 4010003 (2019).
[17] Z. Jaworski, T. Spychaj, A. Story, and G. Story, Rev. Chem. Eng. **37** (2021).10.1515/revce-2020-0016
[18] P. C. F. Møller, J. Mewis, and D. Bonn, Soft Matter **2**, 274 (2006).
[19] M. Dinkgreve, J. Paredes, M. M. Denn, and D. Bonn, J. Non-Newtonian Fluid Mech. **238**, 233 (2016).
[20] M. Dinkgreve, M. M. Denn, and D. Bonn, Rheol. Acta **56**, 189 (2017).
[21] R. B. Bird, R. C. Armstrong, and O. Hassager, *Dynamics of Polymeric Liquids: Volume 1, Fluid Mechanics*, 2nd ed. (Wiley, New York, 1987).
[22] C. W. Macosko, *Rheology: Principles, Measurements and Applications* (VCH, New York, 1994).
[23] R. G. Larson, *The Structure and Rheology of Complex Fluids*, Topics in Chemical Engineering (Oxford University Press, Oxford, 1999).
[24] D. I. Verrelli and A. R. Kilcullen, Adv. Condens. Matter Phys. **2016**, 1716598 (2016).
[25] E. Guazzelli and O. Pouliquen, J. Fluid Mech. **852**, P1 (2018).
[26] R. Seto and G. G. Giusteri, J. Fluid Mech. **857**, 200 (2018).
[27] J. F. Hutton, Rheol. Acta **14**, 979 (1975).
[28] N. W. Taylor and S. H. Gordon, J. Appl. Polym. Sci. **27**, 4377 (1982).
[29] V. Labiausse, R. Höhler, and S. Cohen-Addad, J. Rheol. **51**, 479 (2007).
[30] F. Ahonguio, L. Jossic, and A. Maginn, J. Non-Newtonian Fluid Mech. **206**, 57 (2014).
[31] M. Habibi, M. Dinkgreve, J. Paredes, M. M. Denn, and D. Bonn, J. Non-Newtonian Fluid Mech. **238**, 33 (2016).
[32] H. de Cagny, M. Fazilati, M. Habibi, M. M. Denn, and D. Bonn, J. Rheol. **63**, 285 (2019).
[33] R. L. Thompson, L. U. R. Sica, and P. R. de Souza Mendez, J. Non-Newtonian Fluid Mech. **261**, 211 (2018).
[34] A. N. Beris, R. C. Armstrong, J. Tsamopoulos, and R. A. Brown, J. Fluid Mech. **158**, 219 (1985).
[35] E. Mitsoulis and J. Tsamopoulos, Rheol. Acta **56**, 231 (2017).
[36] P. Saramito and A. Wachs, Rheol. Acta **56**, 211 (2017).
[37] S. Varchanis, S. J. Haward, C. C. Hopkins, A. Syrakos, A. Q. Shen, Y. Dimakopoulos, and J. Tsamopoulos, Proc. Natl. Acad. Sci. U.S.A. **117**, 12611 (2020).
[38] P. Saramito, J. Non-Newtonian Fluid Mech. **158**, 154 (2009).
[39] J. R. Seth, L. Mohan, C. Locatelli-Champagne, M. Cloitre, and R. T. Bonnecaze, Nat. Mater. **10**, 838 (2011).
[40] G. J. Donley, J. R. de Bruyn, G. H. McKinley, and S. A. Rogers, J. Non-Newtonian Fluid Mech. **264**, 117 (2019).
[41] C. J. Dimitriou and G. H. McKinley, J. Non-Newtonian Fluid Mech. **265**, 116 (2019).
[42] K. Kamani, G. J. Donley, and S. A. Rogers, Phys. Rev. Lett. **126**, 218002 (2021).
[43] R. Benzi, T. Divoux, C. Barentin, S. Manneville, M. Sbragaglia, and F. Toschi, Phys. Rev. Lett. **127**, 148003 (2021).
[44] N. Cuny, R. Mari, and E. Bertin, Phys. Rev. Lett. **127**, 218003 (2021).
[45] W. H. Herschel and R. Bulkley, Koll. Zeit. **39**, 291 (1926).
[46] E. C. Bingham, Bull. Bur. Stand. **13**, 309 (1916).
[47] J. G. Oldroyd, Proc. Cambridge Philos. Soc. **43**, 100 (1947).
[48] L. Martinie, H. Buggisch, and N. Willenbacher, J. Rheol. **57**, 627 (2013).
[49] X. Zhang, O. Fadoul, E. Lorenceau, and P. Coussot, Phys. Rev. Lett. **120**, 048001 (2018).
[50] A. Geffrault, H. Bessaies-Bey, N. Roussel, and P. Coussot, J. Rheol. **65**, 887 (2021).
[51] G. Ovarlez, Q. Barral, and P. Coussot, Nat. Mater. **9**, 115 (2010).
[52] L. U. R. Sica, P. R. de Souza Mendes, and R. L. Thompson, Soft Matter **16**, 7576 (2020).
[53] R. L. Thompson and P. R. de Souza Mendez, J. Rheol. **64**, 615 (2020).

[54] See Supplemental Material at http://link.aps.org/supplemental/10.1103/PhysRevLett.129.068002 for details of data collection and analysis are described. Also included are additional data that support the experimental methods and main findings of the study, which includes Ref. [55].
[55] K. Ahnert and M. Abel, Comput. Phys. Commun. **177**, 764 (2007).
[56] M. G. Hansen and F. Nazem, Trans. Soc. Rheol. **19**, 21 (1975).
[57] R. L. Crawley and W. W. Graessley, Trans. Soc. Rheol. **21**, 19 (1977).
[58] C. M. Vrentas and W. W. Graessley, J. Non-Newtonian Fluid Mech. **9**, 339 (1981).
[59] J. S. Vrentas, D. C. Venerus, and C. M. Vrentas, J. Non-Newtonian Fluid Mech. **40**, 1 (1991).
[60] D. C. Venerus and H. Kahvand, J. Rheol. **38**, 1297 (1994).
[61] D. C. Venerus, J. Rheol. **49**, 277 (2005).
[62] D. C. Venerus and R. Nair, J. Rheol. **50**, 59 (2006).
[63] T. Schweizer and A. Bardow, Rheol. Acta **45**, 393 (2006).
[64] C. S. Dutcher and D. C. Venerus, J. Non-Newtonian Fluid Mech. **150**, 154 (2008).
[65] R. Mari, R. Seto, J. F. Morris, and M. M. Denn, Proc. Natl. Acad. Sci. U.S.A. **112**, 15326 (2015).
[66] A. Montesi, A. A. Peña, and M. Pasquali, Phys. Rev. Lett. **92**, 058303 (2004).
[67] T. Liu, F. Khabaz, R. T. Bonnecaze, and M. Cloitre, Soft Matter **14**, 7064 (2018).
[68] F. Khabaz, B. F. Di Dio, M. Cloitre, and R. T. Bonnecaze, J. Rheol. **65**, 241 (2021).
[69] S. Jamali, G. H. McKinley, and R. C. Armstrong, Phys. Rev. Lett. **118**, 048003 (2017).
[70] D. J. Pine, J. P. Gollub, J. F. Brady, and A. M. Leshansky, Nature (London) **438**, 997 (2005).
[71] T. Kawasaki and L. Berthier, Phys. Rev. E **94**, 022615 (2016).